Optical Materials 96 (2019) 109340

Contents lists available at ScienceDirect

Optical Materials

journal homepage: www.elsevier.com/locate/optmat

# Rich reddish-orange emitting PBTNAPr glasses for laser applications

B.C. Jamalaiah[a,*], G. Viswanadha[a], K. Venkata Rao[b]

[a] Department of Physics, Rajeev Gandhi Memorial College of Engineering and Technology (Autonomous), Nandyal, 518501, Andhra Pradesh, India
[b] Department of Physics, S.B.V.R. Degree College, Badvel, 516227, Andhra Pradesh, India

ARTICLE INFO

*Keywords:*
Lead borate glasses
Solid state lasers
Judd-Ofelt analysis
Photoluminescence

ABSTRACT

Lead borate oxyfluoride glasses containing different amounts of $PrF_3$ with composition $PbO–B_2O_3–TeO_2–NaF–AlF_3$-$PrF_3$ were prepared and characterized for visible and fiber lasers. The amorphous phase and compositional analysis were carried out through powder X-ray diffraction and Fourier transform infrared spectra, respectively. Using the room temperature optical absorption spectra, the spectroscopic properties were determined applying the modified Judd-Ofelt theory. The photoluminescence excitation spectral studies obtained by controlling the emission through $Pr^{3+}$: $^1D_2 \rightarrow {}^3H_4$ (604 nm) transition shows prominent excitation band positioned at ~448 nm ($^3H_4 \rightarrow {}^3P_2$). Upon 448 nm excitation, the studied glasses exhibit an intense emission through $^1D_2 \rightarrow {}^3H_4$ (604 nm) transition along with feeble emissions from $^3P_1$ and $^3P_0$ metastable levels to the inner energy levels. The emission spectra show a shift towards longer wavelengths (called the red-shift) with increase of $PrF_3$ content. The luminescence decay time of $^1D_2$ emission level was found decreased with increase of $PrF_3$ content. The quenching of decay time was assigned to the transfer of energy among the excited $Pr^{3+}$ ions at relatively higher $PrF_3$ contents. The experimental results show that the studied glasses with 0.1 mol% of $PrF_3$ could be the suitable candidate to design rich reddish-orange emitting lasers.

## 1. Introduction

The rare earth (RE) ions exhibit efficient fluorescence properties in different solid state host matrices due to their small homogeneous linewidths and several excited states available for optical pumping. Hence, search has been going on to design high efficient solid state host matrices to meet the needs of current technologies. Among the available host matrices, the oxyfluoride based glassy materials have potential applications in various photonic and optoelectronic fields due to broad inhomogeneous bandwidths, large amount of RE ion solubility, relatively large thermal stability, chemical durability and high luminescence efficiency. Now-a-days, the trivalent RE ions activated oxyfluoride glassy materials have been extensively investigated for solid state lasers, optical amplifiers, scintillators, etc. They also find wide range of applications in the field of fiber laser cooling [1–5].

In general, an intrinsic borate glass would not acts as a good optical gain medium for $RE^{3+}$ ions due to the presence of multi-phases, relatively high phonon energy (~2000 $cm^{-1}$) and considerably low moisture resistant. However, the lead borate based multi-component oxyfluoride glassy matrices can be used as the best choice compared to other silicate, phosphate, tellurite hosts, etc. The formation of multi-phases can be avoided by converting $BO_3$ borate structural units into $BO_4$ units with the addition of suitable network modifiers and alkali ions to the borate network. It is well known fact that the addition of small amounts of heavy-metal oxides such as PbO and $Bi_2O_3$ to the borate network reduces the melting temperature while the addition of fluoride content minimizes the phonon energy [6–8]. The studied $PbO–B_2O_3–TeO_2–NaF–AlF_3$ (PBTNA) glass host could have good optical quality in UV–Vis–NIR regions due to the presence of small amounts of $TeO_2$ in addition to low melting point, low phonon energy and good thermal stability [9].

Among the available trivalent RE ions, the $Pr^{3+}$ ions have potential applications in the fields of display technology, optical data storage and medical diagnosis owing to their diverse energy level structure which contains different metastable quantum levels such as $^3P_2$, $^3P_1$, $^3P_0$, $^1D_2$ and $^1G_4$ resulting proficient emission in visible, near and mid infrared regions [10,11]. The $Pr^{3+}$ -activated upconversion lasers are favourable to design 1.3 μm optical fiber amplifiers [12]. However, the $Pr^{+3}$ -doped oxyfluoride based glassy materials with relatively low phonon energy would be the best alternative for visible and fiber lasers. Usually, the standard Judd-Ofelt (J-O) theory [13,14] fails to determine the intensity parameters of $Pr^{3+}$ -doped glassy materials due to small difference in energy between the $4f^2$ ground level and the ($4f^{n-1}5d$) excited levels of $Pr^{3+}$ ion. A brief idea about the failure of standard J-O

* Corresponding author.
*E-mail address:* bcjphysics@gmail.com (B.C. Jamalaiah).

https://doi.org/10.1016/j.optmat.2019.109340
Received 20 July 2019; Received in revised form 5 August 2019; Accepted 20 August 2019

theory and the application of modified J-O theory has been described in our previous work [6].

The present investigation includes the analysis of spectroscopic and laser characteristic properties of different amounts of $PrF_3$ activated PBTNA glassy materials. The intensity parameters were evaluated following the modified J-O theory. The colour of emitted luminescence was discussed using the Commission International de l'Eclairage (CIE) chromaticity co-ordinates evaluated from the emission spectral profiles. The energy transfer processes accountable for the luminescence quenching and the lifetime shortening were discussed. The applicability of PBTNAPr glasses for laser hosts for reddish-orange emission was also explained.

## 2. Experimental

### 2.1. Materials and method of preparation

Trivalent praseodymium doped lead borate oxyfluoride (PBTNAPr) glasses with composition 30 PbO + (50 – $x$) $B_2O_3$ + 5 $TeO_2$ + 10 NaF + 5 $AlF_3$ + $x$ $PrF_3$ where $x$ = 0, 0.1, 0.5, 1.0 and 2.0 mol% were synthesized by melt-quenching technique. The homogeneous powder of about 20 g batch from the raw materials of PbO (98.0%, Himedia), $H_3BO_3$ (≥99.5%, Merk), $TeO_2$ (≥99%, Sigma Aldrich), NaF (≥97%, Merk), $AlF_3$ (97%, Sigma Aldrich) and $PrF_3$ (≥99.9%, Alfa aesar) were melted at 900 °C for 1 h using alumina crucible. The melt was quenched in air using pre-heated brass plates and annealed at 350 °C for 10 h to eliminate the glass fractures occurred due to thermal stress. Finally, the glass samples were cooled to room temperature and polished for optical quality with 0.16 ± 0.01 cm thickness. For convenience, the samples were referred as PBTNAPr0, PBTNAPr01, PBTNAPr05, PBTNAPr10 and PBTNAPr20 glasses for $x$ = 0, 0.1, 0.5, 1.0 and 2.0 mol%, respectively.

### 2.2. Characterization

The densities of prepared glasses were determined applying the Archimedean principle using double distilled water as buoyant fluid. The index of refraction was determined with Abbes' refractometer using sodium vapour lamp (λ = 5893 Å) as source of light and 1-bromo-napthalene ($C_{10}H_7Br$) as cementing material. The thermal properties of synthesized glasy materials were analysized with Shimadzu DTG-60H DTA-TG apparatus under $N_2$ ambiance at 10 °C/min. heating rate. The X-ray diffraction profiles were obtained using RIGAKU; Miniflex-600 X-ray diffractometer with CuKα1 radiation of wavelength 1.5406 Å. The Fourier transforms infrared (FTIR) absorption analysis (KBr technique) was carried out on PerkinElmer Spectrum one: FT-IR spectrometer with a resolution of 1.0 $cm^{-1}$. The Optical absorption studies were carried out on PerkinElmer Lambda 950 spectrophotometer with a spectral resolution of 0.1 nm. The photoluminescence excitation and the visible luminescence properties were recorded on Hitachi-F7000 Fluorescence spectrophotometer using xenon flash lamp as source of light. The luminescence decay studies were taken on Jobin YVON Fluorolog-3 fluorimeter with xenon flash lamp as a radiation source. All the optical measurements were performed at room temperature.

## 3. Results and discussion

### 3.1. Basic properties

The addition of $PrF_3$ to the PBTNAPr glasses modifies a few physical and optical properties such as density, index of refraction, dielectric constant, reflection loss and molar volume. A few significant properties of PBTNAPr glasses are evaluated [15] and presented in Table 1. The density (ρ) of a material describes its atomic or molecular compactness. For the titled glasses, the magnitudes of density and refractive index (n) increase with increase of $PrF_3$ content. The variation of density and index of refraction versus $PrF_3$ content are described in Fig. 1(a) and (b). The average molecular weight increases with the addition of $PrF_3$ content. Fig. 1(c) shows the variation of average molecular weight versus $PrF_3$ content in PBTNAPr glasses.

**Table 1**
Comparison of some of the basic properties such as density (ρ, g/$cm^3$), refractive index (n), $Pr^{3+}$ ions concentration (N × $10^{-20}$ ions/$cm^3$), dielectric constant (K) reflection losses (R, %), average molecular weight ($\bar{M}$, g), molar volume ($V_m$, $cm^3$) and optical band gap energy ($E_{opt}$, eV) of PBTNAPr glasses.

| Property | PBTNAPr0 | PBTNAPr01 | PBTNAPr05 | PBTNAPr10 | PBTNAPr20 |
|---|---|---|---|---|---|
| ρ | 5.423 | 5.485 | 5.576 | 5.615 | 5.686 |
| n | 1.540 | 1.547 | 1.556 | 1.567 | 1.574 |
| N | – | 0.239 | 1.213 | 2.433 | 4.829 |
| K | 2.372 | 2.396 | 2.418 | 2.459 | 2.477 |
| R | ~5.000 | ~5.000 | ~5.000 | ~5.000 | ~5.000 |
| $\bar{M}$ | 118.143 | 118.276 | 118.786 | 119.425 | 120.702 |
| $V_m$ | 21.778 | 21.568 | 21.341 | 21.264 | 22.228 |
| $E_{opt}$ | 2.642 | 2.445 | 2.169 | 1.820 | 1.590 |

It is well known that the structure compactness of materials has been expressed in terms of molar volume ($V_m$), which can be defined as the ratio of average molecular weight ($\bar{M}$) and density (ρ) of a material. The molar volume of PBTNAPr glasy materials decrease gradually with the addition of $PrF_3$ content as described in Fig. 1(d). The increased compactness of atoms or molecules, refractive index and average molecular weight and the decreased molar volume affects the luminescence properties of PBTNAPr glasses. Further, the reflection losses are found to be ~5.000% which indicates that a major contribution of incident light energy transmits through PBTNAPr glasses showing high transparency.

### 3.2. Thermal analysis

The glass transition temperature ($T_g$), onset crystallization temperature ($T_x$), bulk crystallization temperature ($T_c$) and melting temperature ($T_m$) plays a key role in investigating thermal stability, ΔT (= $T_x$–$T_g$) and glass-forming tendency which can be expressed in terms of Herby number, H (= $T_c$–$T_g$/$T_m$–$T_c$) [16]. The knowledge of these parameters is essential in fabricating solid-state lasers and fibers. Further, a glass with high thermal stability and small temperature interval between $T_m$ and $T_c$ are favourable for lasers and fibers [17]. The DTA pattern of PBTNAPr0 glass shown in Fig. 2 reveals a considerably small endothermic peak at around 150 °C due to the borate phase transformation from $BO_3$ to $BO_4$ groups [18] resulting the absence of multi-phases.

It is known that the host matrices with ΔT > 100 °C are more favourable for laser applications. The thermal stability of PBTNAPr0 glass is comparable to LABS [2] and TWG [15] glasses. Additionally, the host matrices with reasonably large value of Herby number show large glass-forming tendency. In the present investigation, the Herby number is found to be 3.327 for PBTNAPr0 glass and it is close to TWG [15] glass. The thermal stability and Herby number suggests that the PBTNAPr glasses are suitable to draw fibers without devitrification. The studied glasses show improved thermal properties over TWG10 [15] glass. A comparison of thermal properties of studied glasses with our previous work on TWG [15] glasses is presented in Table 2.

### 3.3. XRD and FTIR studies

The amorphous phase of PBTNAPr glasses has been confirmed from the powder XRD patterns. For this purpose, the prepared glasy materials are ground well with a particle size of the order of 53 μm. The XRD patterns of investigated glass samples contain a broad diffuse scattering from 2θ = 15° to 2θ = 38°. This is the one of the characteristic features of long-range structural disorder indicating the amorphous phase of glasses under investigation. Therefore, the PBTNAPr glasses are pure amorphous and they are free from crystalline phases. The XRD patterns of PBTNAPr0 and PBTNAPr10 glasses are described in Fig. 3.

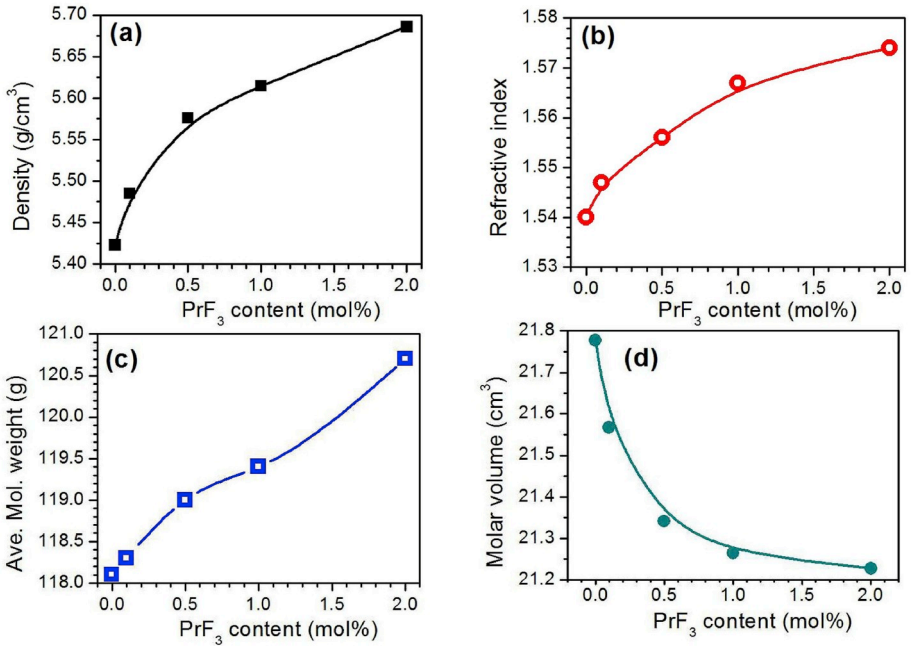


**Fig. 1.** Variation of density (a), refractive index (b), average molecular weight (c) and molar volume (d) as a function of $PrF_3$ content in PBTNAPr glasses.

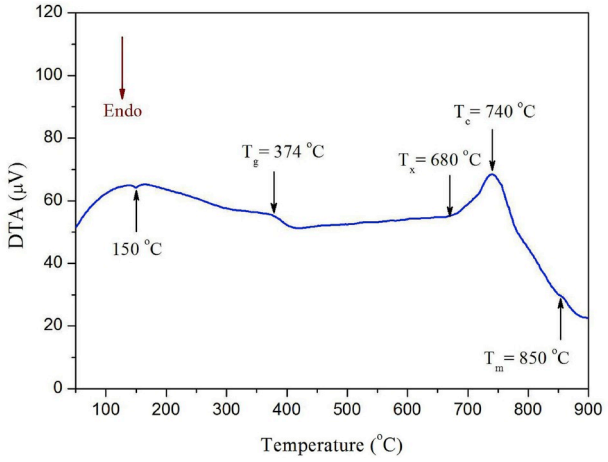


**Fig. 2.** DTA profile of PBTNAPr0 glass.

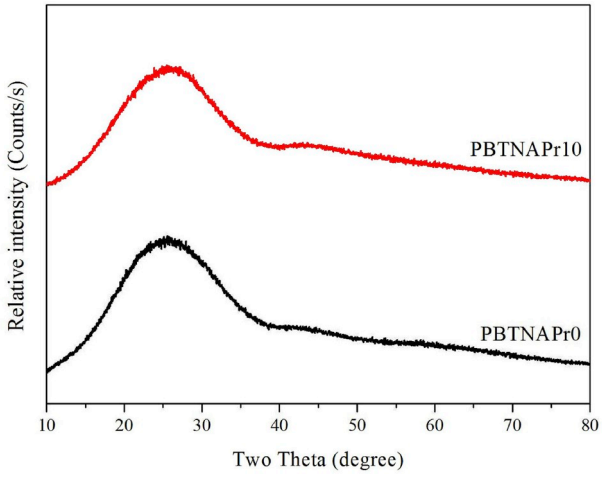


**Fig. 3.** XRD patterns of PBTNAPr glasses.

**Table 2**
Thermal properties of different host glasses.

| Parameter | PBTNAPr0 [Present work] | TWG10 [15] |
|---|---|---|
| Glass transition temperature, $T_g$ (°C) | 374 | 385 |
| Onset crystallization temperature, $T_x$ (°C) | 680 | 437 |
| Bulk crystallization temperature, $T_c$ (°C) | 740 | 511 |
| Melting temperature, $T_m$ (°C) | 850 | 560 |
| Thermal stability, ΔT (°C) | 306 | 123 |
| Herby number, H | 3.327 | 2.57 |

The presence of various vibrational modes of glass network and metallic cations has been confirmed from the FTIR spectrum of PBTNAPr0 glass and it is described in Fig. 4. This spectrum reveals seven IR active modes at about 3430, 2920, 1630, 1358, 1005, 695 and 490 $cm^{-1}$. A broad IR band peaked at ~3430 $cm^{-1}$ and ~2920 $cm^{-1}$ belongs to the symmetric stretching vibrations of $OH^-$ group [19]. The IR bands noticed at ~1630 and ~1358 $cm^{-1}$ arises from the *ortho-*

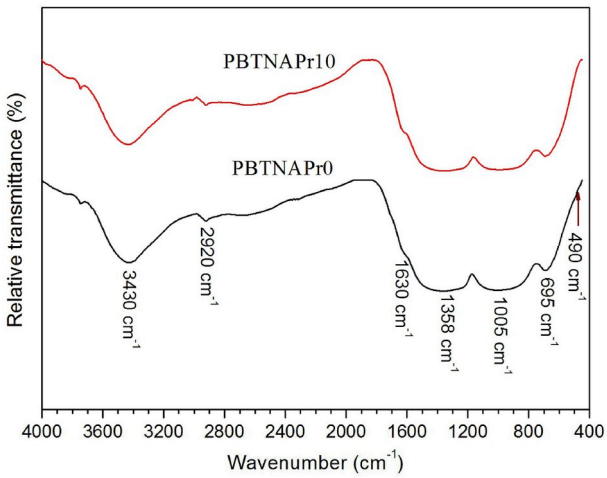


**Fig. 4.** FTIR spectra of PBTNAPr glasses.

borate group and they can be attributed to the asymmetric stretching vibrations of B–O bonds. The IR band with peak maximum at ~1005 $cm^{-1}$ occurs from the di-borate group and it is ascribed to the stretching vibrations of B–O bonds. The IR band positioned at ~695 $cm^{-1}$ happens from the $BO_4$ group and it is assigned to the B–O–B bending vibrations. The IR band observed at ~490 $cm^{-1}$ is credited to the O–B–O bending vibrations associated with covalent Pb–O vibrations [20,21]. The IR active modes of PBTNAPr0 glass are suitably matched with LiPbAlB [22] and PTBDy [23] glasses.

The FTIR spectral analysis is also useful in determining the phonon energy and $OH^-$ content which affects the optical losses and quantum efficiency [24]. The energy corresponding to the low intense IR transmittance band signifies the phonon energy of amorphous material [25]. From the FTIR spectrum shown in Fig. 4, the phonon energy is noted as nearly 1005 $cm^{-1}$ for PBTNAPr glass and it is close to LiPbAlB [22] and PTBDy [23] glasses. The presence of $OH^-$ content in any glasy material has been estimated in terms coefficient of $OH^-$ and it can be evaluated using the equation, $\alpha_{OH} = \ln\left(\frac{T_O}{T_D}\right) \times l^{-1}$, where $T_O$ and $T_D$ represents the highest transmission and the glass transmission at 3000 $cm^{-1}$, respectively [26]. For PBTNAPr0 glass, the magnitude of $\alpha_{OH}$ is estimated to be 66.81 ppm and it is close to ZnAlBiB glass (65.48 ppm) [27] and found lower than LBTAF (123.00 ppm) [28], KBS (133 ppm) [29], $GeS_2$ (175.5 ppm) [30] and LHG-8L (128 ppm) [31] glasses. Considerably small $\alpha_{OH}$ and low phonon energy of PBTNAPr glass suggests that they are more suitable for laser applications.

### 3.4. Absorption spectral analysis

#### 3.4.1. Optical absorption spectra

The spectroscopic properties and the J-O intensity parameters of PBTNAPr glasses have been obtained from the optical absorption spectra. The absorption pattern of PBTNAPr0 glass shows fundamental absorption at around 435 nm (or ~2.851 eV). In visible region, the absorption spectra of $Pr^{3+}$ -doped PBTNAPr glasses consist of $^3H_4 \rightarrow {}^3P_2$, $^3P_1$, $^3P_0$, $^1D_2$ transitions positioned at around 447, 472, 485 and 593 nm, respectively. In infrared region, they reveal $^3H_4 \rightarrow {}^1G_4$, $^3F_4$, $^3F_3$, $^3F_2$ and $^3H_6$ transitions with peak maximum at around 1009, 1445, 1529, 1936 and 2358 nm, respectively [32]. The absorption spectral profiles of PBTNAPr0, PBTNAPr10 and PBTNAPr20 gasses are shown in Fig. 5. From the absorption spectra one can notice that with increase of $PrF_3$ content, the absorbance of observed absorption transitions increase and their positions do not alter due to the symmetric ligand field environment around the $Pr^{3+}$ ions indicating the homogeneous distribution of $Pr^{3+}$ ions in PBTNAPr glasses. Fig. 6 shows the variation of absorbance of $^3H_4 \rightarrow {}^3P_2$ (448 nm) and $^3H_4 \rightarrow {}^3F_3$ (1529 nm) transitions versus $PrF_3$ content.

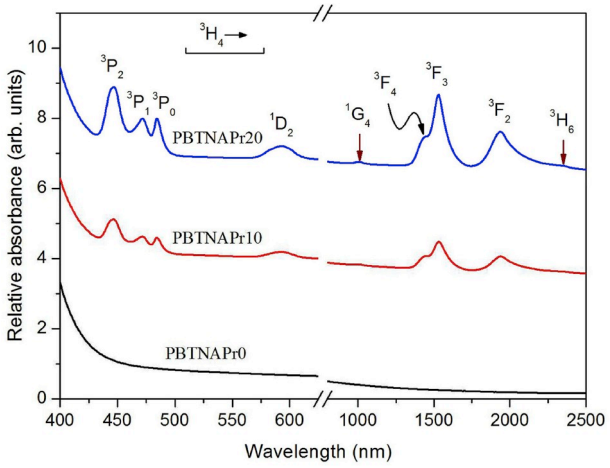


**Fig. 5.** Absorption spectra of PBTNAPr glasses.

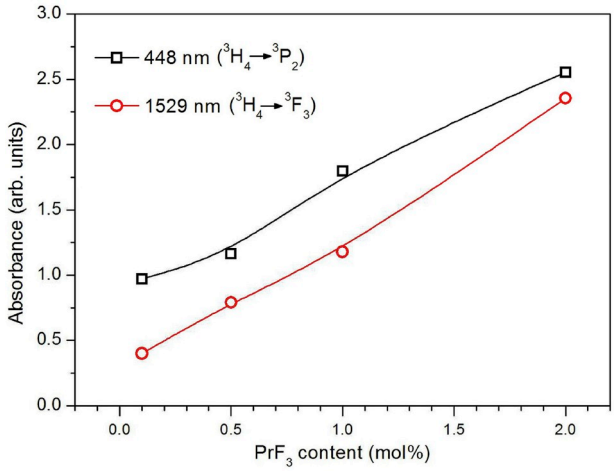


**Fig. 6.** Absorbance vs. $PrF_3$ content for $^3H_4 \rightarrow {}^3P_2$, $^3F_3$ transitions in PBTNAPr glasses.

#### 3.4.2. Bonding character

The positions of observed absorption transitions in PBTNAPr glasses are found deviate slightly from their positions in aqua-ion host due to the nature of $Pr^{3+}$ bonding with the surrounding ligands. This deviation in band positions is expressed in terms of nephelauxetic ratio and it is defined as the ratio of positions of absorption transitions noticed in the studied medium ($\bar{\nu}_c$) and in aqua-ion medium ($\bar{\nu}_a$) [i.e., $\beta = (\bar{\nu}_c/\bar{\nu}_a]$. The bonding nature (either covalent or ionic) has been identified from the bonding parameter, $\delta = \left[\left(1 - \bar{\beta}/\beta\right) \times 100\right]$, where $\bar{\beta}$ is the average nephelauxetic ratio [33]. The positive value of δ is an indication for covalent nature, while the negative is for ionic nature of $Pr^{3+}$ and ligand bonds. The absorption band positions, nephelauxetic ratios and the bonding parameters for individual absorption transitions are listed in Table 3. The mean value of δ (nearly +0.008) reveals covalent nature for $Pr^{3+}$ and ligand bond in PBTNAPr glasses.

The degree of covalent nature of $Pr^{3+}$-ligand bonds has been expressed in terms of covalent character, $C_{cov}$ (%) = exp [–0.25 $(\Delta\chi)^2$] × 100, where Δχ represents the electronegativity of host matrix [34]. The $C_{cov}$ is found to be 57.28%, 57.04%, 56.76% and 56.17% for PBTNAPr01, PBTNAPr05, PBTNAPr10 and PBTNAPr20 glasses, respectively. The covalent character of the studied glasses is close to PTBPr glass [6]. In the present investigation, the covalent character of PBTNAPr glasses predominate the ionic character resulting large rigidity. The decrease in $C_{cov}$ with increase of $PrF_3$ content indicates a feeble decrease in rigidity of PBTNAPr glasses.

**Table 3**
Absorption peak positions in PBTNAPr glasses ($\bar{\nu}_c$) and in aqua-ion ($\bar{\nu}_a$) and nephelauxetic ratios (β) and bonding parameters (δ) for observed transitions.

| Transition | Peak maximum ($cm^{-1}$) | | β | δ |
|---|---|---|---|---|
| | $\bar{\nu}_c$ | $\bar{\nu}_a$ | | |
| $^3H_4 \rightarrow {}^3P_2$ | 22371 | 22532 | 0.992 | 0.008 |
| $^3H_4 \rightarrow {}^3P_1$ | 21186 | 21330 | 0.993 | 0.008 |
| $^3H_4 \rightarrow {}^3P_0$ | 20618 | 20706 | 0.996 | 0.008 |
| $^3H_4 \rightarrow {}^1D_2$ | 16863 | 16840 | 1.001 | 0.008 |
| $^3H_4 \rightarrow {}^1G_4$ | 9911 | 9885 | 1.003 | 0.008 |
| $^3H_4 \rightarrow {}^3F_4$ | 6920 | 6975 | 0.992 | 0.008 |
| $^3H_4 \rightarrow {}^3F_3$ | 6540 | 6540 | 1.000 | 0.008 |
| $^3H_4 \rightarrow {}^3F_2$ | 5165 | 5149 | 1.003 | 0.008 |
| $^3H_4 \rightarrow {}^3H_6$ | 4241 | 4496 | 0.943 | 0.009 |
| Average nephelauxetic ratio, $\bar{\beta}$ = 0.992 | | | | |
| Mean bonding parameter, δ = 0.008 | | | | |

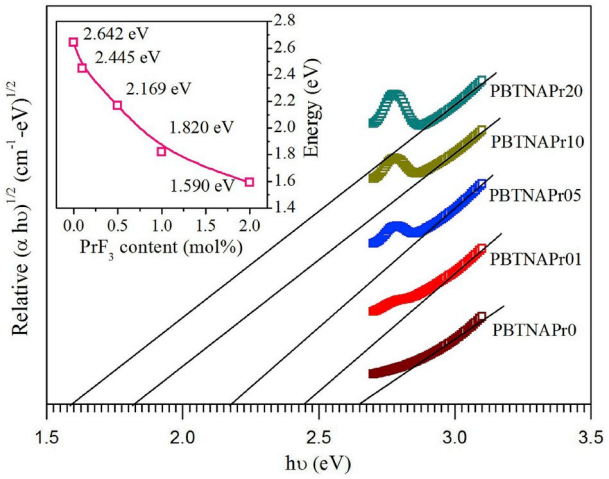


**Fig. 7.** Tauc's plots for direct allowed transitions in PBTNAPr glasses. Inset is the variation of optical band gap energy as a function of $PrF_3$ content.

### 3.4.3. Optical band gap energy

The knowledge of optical band gap energy ($E_{opt}$) is one of the noteworthy parameters for photonic devices. Mott and Davis [35] established a relation to the optical band gap energy and it is given by

$$\alpha \,.\, (h\nu) \;=\; A\,(h\nu - E_{opt})^{q} \qquad (1)$$

where α is the absorption coefficient near the fundamental absorption edge, $h\nu$ is the photon energy, A is an energy independent parameter and q = 2 for indirect allowed, q = 3 for indirect forbidden, q = ½ for direct allowed and q = ⅓ for direct forbidden transitions. Since the optical band gap energy for direct allowed transitions play a vital role in photonic devices, the present research work is confined to evaluate direct band gap energy for allowed transitions only. The magnitude of $E_{opt}$ has been determined by extrapolating the linear region of $(\alpha.h\nu)^{1/2}$ versus photon energy (hν) curve (known as Tauc's plot) to meet hν axis at $(\alpha.h\nu)^{1/2} = 0$. The Tauc's plots for direct allowed transitions of PBTNAPr glasses are illustrated in Fig. 7. The values of $E_{opt}$ are found to be 2.642, 2.445, 2.169, 1.820 and 1.590 eV for PBTNAPr0, PBTNAPr01, PBTNAPr05, PBTNAPr10 and PBTNAPr20 glasses, respectively. The value of $E_{opt}$ decrease gradually with increase of $PrF_3$ content due to the formation of additional quantum states and slight structural modifications.

### 3.4.4. Intensity parameters

The intensity of observed absorption transitions is mentioned in terms of dimensionless parameters, known as experimental oscillator strengths ($f_{exp}$) and they can be evaluated from the area under the absorption bands. Some of the absorption transitions are more perceptive to the host matrix and are known as hypersensitive transitions obeying $\Delta S = 0, \Delta L \leq \pm 2, \Delta J \leq \pm 2$ selection rules and characterized by large magnitude of experimental oscillator strengths [36]. From the evaluated values of experimental oscillator strengths presented in Table 4, one can notice that the $^3H_4 \rightarrow {}^3P_2$ transition is hypersensitive one. In our previous work on PTBPr glasses [6], we have applied a modified J-O theory to evaluate the laser characteristic parameters. According to modified J-O theory, the electric dipole linestrengths can be calculated using the formula shown below [37].

$$S_{ed}(\psi J,\ \psi' J') = e^2 \sum_{\lambda = 2,4,6} \Omega'_{\lambda} \left[1 + 2\gamma\left(E_{\psi J} + E_{\psi' J'} - 2E_f^0\right)\right] \langle \psi J \| U^{\lambda} \| \psi' J' \rangle^2 \qquad (2)$$

where $\Omega'_{\lambda}$ are the J-O intensity parameters from the modified model, $E_{\psi J}$ is the energy of ground level, $E_{\psi' J'}$ is the energy of excited level and

**Table 4**
Comparison of oscillator strengths ( × $10^{-6}$) and root mean square deviations ($\delta_{rms} \times 10^{-6}$) in PBTNAPr glasses.

| Transition | PBTNAPr01 | | PBTNAPr05 | | PBTNAPr10 | | PBTNAPr20 | |
|---|---|---|---|---|---|---|---|---|
| | $f_{exp}$ | $f_{cal}$ | $f_{exp}$ | $f_{cal}$ | $f_{exp}$ | $f_{cal}$ | $f_{exp}$ | $f_{cal}$ |
| $^3H_4 \rightarrow {}^3P_2$ | 3.379 | 3.103 | 2.594 | 3.002 | 2.767 | 2.788 | 2.861 | 2.748 |
| $^3H_4 \rightarrow {}^3P_1$ | 0.654 | 1.586 | 0.682 | 1.556 | 0.559 | 1.180 | 0.615 | 0.988 |
| $^3H_4 \rightarrow {}^3P_0$ | 0.862 | 1.545 | 0.791 | 1.516 | 0.546 | 1.150 | 0.530 | 0.963 |
| $^3H_4 \rightarrow {}^1D_2$ | 1.243 | 0.836 | 0.938 | 0.811 | 0.619 | 0.746 | 0.724 | 0.744 |
| $^3H_4 \rightarrow {}^1G_4$ | 0.180 | 0.208 | 0.178 | 0.202 | 0.198 | 0.187 | 0.256 | 0.186 |
| $^3H_4 \rightarrow {}^3F_4$ | 1.534 | 2.279 | 1.512 | 2.207 | 1.525 | 2.072 | 1.710 | 2.085 |
| $^3H_4 \rightarrow {}^3F_3$ | 4.157 | 3.682 | 4.092 | 3.584 | 3.637 | 3.252 | 3.482 | 3.242 |
| $^3H_4 \rightarrow {}^3F_2$ | 1.451 | 1.481 | 1.508 | 1.542 | 1.183 | 1.206 | 1.539 | 1.554 |
| $^3H_4 \rightarrow {}^3H_6$ | 0.347 | 0.392 | 0.345 | 0.379 | 0.333 | 0.353 | 0.354 | 0.348 |
| $\delta_{rms}$ | ± 0.512 | | ± 0.497 | | ± 0.367 | | ± 0.246 | |

$E_f^0$ is the energy corresponding to the centre of gravity of 4*f* configuration. The parameter $\gamma = \frac{1}{2}[E(4f.\,5d) - E(4f)]$, is known as a fitting parameter. In case of $Pr^{3+}$ ions in any glass matrix, the magnitudes of $E_f^0$ and $\gamma$ are of the order of ~9940 and $1.0 \times 10^{-5}\,cm^{-1}$, respectively. To execute the modified J-O model, the host insensitive squared reduced matrix elements ($\|U^{\lambda}\|^2$) from the standard J-O theory have been modified by multiplying with $[1 + 2\gamma(E_{\psi J} + E_{\psi' J'} - 2E_f^0)]$. The standard and modified values of $\|U^{\lambda}\|^2$ for the observed absorption transitions of $Pr^{3+}$ ions are summarized in Table 5. Theoretically calculated oscillator strengths ($f_{cal}$) and hence the three phenomenological J-O intensity parameters ($\Omega_{\lambda=2,4,6}$) have been obtained applying a least squares fit approach. Reasonably small root mean square deviation ($\delta_{rms}$) indicates good fit between $f_{exp}$ and $f_{cal}$ and the best set of $\Omega_{\lambda=2,4,6}$ intensity parameters. A comparison of experimental and calculated oscillator strengths for the observed transitions of PBTNAPr glasses is given in Table 4.

In the present investigation for PBTNAPr01, PBTNAPr05 and PBTNAPr10 glasses, the J-O intensity parameters are found to be in the order $\Omega_2 < \Omega_4 < \Omega_6$ while for PBTNAPr20 glass they follow a trend $\Omega_2 > \Omega_4 < \Omega_6$. The deviation in trend of intensity parameters in a given host matrix is due to the experimental limitations only. The $\Omega_2$ intensity parameters of PBTNAPr01 glass is very close to those reported for LiPbAlB-E [22], BPGBPr [38] and BLiPbP [39] glasses. A comparison of $\Omega_\lambda$ intensity parameters for different host glasses containing $Pr^{3+}$ ions is presented in Table 6. The magnitudes of $\Omega_4$ and $\Omega_6$ intensity parameters decrease gradually with increase of $PrF_3$ content while the magnitude of $\Omega_2$ intensity parameter vary randomly due to the large magnitudes of oscillator strengths and squared reduced matrix elements. The variation of $\Omega_\lambda$ intensity parameters as a function of $PrF_3$ content is described in Fig. 8.

The $\Omega_\lambda$ parameters have been used to know the local site symmetry around the active ion, the covalent character of metal-ligand bond, the

**Table 5**
Squared reduced matrix elements for the observed absorption transitions of $Pr^{3+}$ ions.

| Transition | Squared reduced matrix elements, $\|U^{\lambda}\|^2$ | | | | | |
|---|---|---|---|---|---|---|
| | Standard J-O theory | | | Modified J-O theory | | |
| | $\|U^2\|^2$ | $\|U^4\|^2$ | $\|U^6\|^2$ | $\|U^2\|^2$ | $\|U^4\|^2$ | $\|U^6\|^2$ |
| $^3H_4 \rightarrow {}^3P_2$ | ~0 | 0.0362 | 0.1355 | ~0 | 0.0382 | 0.1429 |
| $^3H_4 \rightarrow {}^3P_1$ | 0 | 0.1707 | 0 | 0 | 0.1760 | 0 |
| $^3H_4 \rightarrow {}^3P_0$ | 0 | 0.1728 | 0 | 0 | 0.1762 | 0 |
| $^3H_4 \rightarrow {}^1D_2$ | 0.0026 | 0.0170 | 0.0520 | 0.0025 | 0.0161 | 0.0491 |
| $^3H_4 \rightarrow {}^1G_4$ | 0.0012 | 0.0072 | 0.0266 | 0.0009 | 0.0058 | 0.0214 |
| $^3H_4 \rightarrow {}^3F_4$ | 0.0187 | 0.0500 | 0.4849 | 0.0139 | 0.0373 | 0.3616 |
| $^3H_4 \rightarrow {}^3F_3$ | 0.0654 | 0.3469 | 0.6983 | 0.0483 | 0.2561 | 0.5154 |
| $^3H_4 \rightarrow {}^3F_2$ | 0.5089 | 0.4032 | 0.1177 | 0.3616 | 0.2865 | 0.0836 |
| $^3H_4 \rightarrow {}^3H_6$ | 0.0001 | 0.330 | 0.1395 | ~0 | 0.0228 | 0.0966 |

**Table 6**
Comparison of intensity parameters ($\Omega_\lambda \times 10^{-20}$ cm$^2$) and their trend in $Pr^{3+}$ -doped different host matrices.

| S. No. | Host matrix | J-O intensity parameters | | | Trend |
|---|---|---|---|---|---|
| | | $\Omega_2$ | $\Omega_4$ | $\Omega_6$ | |
| 1 | PBTNAPr01 [Present work] | 0.876 | 1.414 | 2.848 | $\Omega_2 < \Omega_4 < \Omega_6$ |
| 2 | PBTNAPr05 [Present work] | 1.003 | 1.378 | 2.732 | $\Omega_2 < \Omega_4 < \Omega_6$ |
| 3 | PBTNAPr10 [Present work] | 0.698 | 1.036 | 2.578 | $\Omega_2 < \Omega_4 < \Omega_6$ |
| 4 | PBTNAPr20 [Present work] | 1.431 | 0.863 | 2.569 | $\Omega_2 > \Omega_4 < \Omega_6$ |
| 5 | LiPbAlB-E [22] | 0.62 | 2.12 | 1.51 | $\Omega_2 < \Omega_4 > \Omega_6$ |
| 6 | BPGBPr [38] | 0.67 | 1.99 | 3.75 | $\Omega_2 < \Omega_4 < \Omega_6$ |
| 7 | BLiPbP [39] | 0.53 | 2.01 | 2.26 | $\Omega_2 < \Omega_4 < \Omega_6$ |

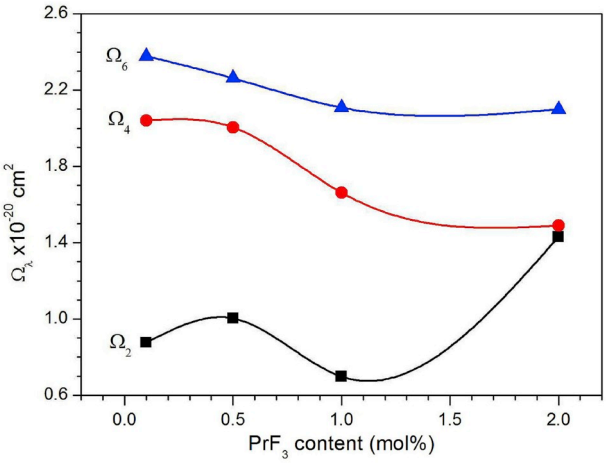


**Fig. 8.** Variation of intensity parameters as a function of $PrF_3$ content in PBTNAPr glasses.

viscosity and the rigidity of host matrix. Since $\Omega_2$ is sensitive to the host matrix, it is directly linked with the local site symmetry and the covalency of metal-ligand bond. Smaller the $\Omega_2$ value more is the local site symmetry and the metal-ligand bond becomes covalent. The evaluated values of $\Omega_2$ indicate that the local site environment around the $Pr^{3+}$ ions is more symmetric and the $Pr^{3+}$-ligand bond is partly covalent. These results are in good agreement with those obtained from bonding parameter and covalent character measurements. The $\Omega_4$ intensity parameter is practically constant and it does not signify any physical parameter. The $\Omega_6$ do not vary appreciably with host environment in most of the glassy matrices and it is a representative of change in viscosity and rigidity of the host matrix. It is known that larger the magnitude of $\Omega_6$ greater is the rigidity and smaller is the viscosity of host matrix. The gradual decrease in $\Omega_6$ indicates that the rigidity of PBTNAPr glasses decrease with increase of $PrF_3$ content due to structural modifications. These observations are similar to that of covalent character results described in section 3.4.2.

### 3.5. Photoluminescence analysis

#### 3.5.1. Excitation spectra

To optimize the concentration of active ions for an intense and potential emission, it is essential to select an appropriate excitation wavelength. In this regard, the photoluminescence excitation has been carried out for all the samples monitoring the emission at 604 nm corresponding to $Pr^{3+}$: $^1D_2 \rightarrow {}^3H_4$ transition. The excitation spectra (normalized w.r.t. the intensity of $^3H_4 \rightarrow {}^3P_2$ transition of PBTNAPr01 glass) presented in Fig. 9 reveal three excitation bands at around 448,

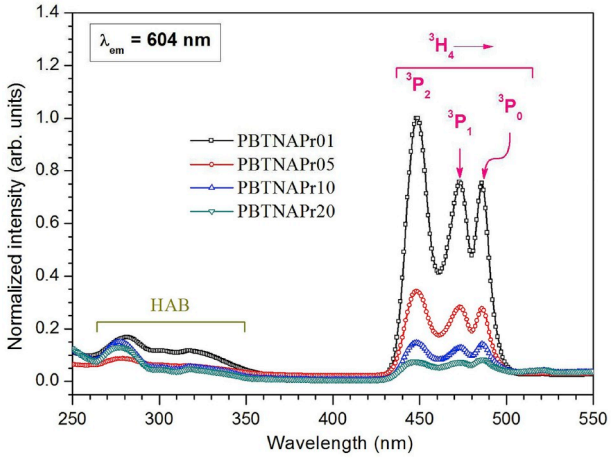


**Fig. 9.** Excitation spectra ($\lambda_{em}$ = 604 nm) of PBTNAPr glasses.

473 and 486 nm corresponding to $^3H_4 \rightarrow {}^3P_2$, $^3H_4 \rightarrow {}^3P_1$ and $^3H_4 \rightarrow {}^3P_0$ transitions, respectively [32]. Among these, the $^3H_4 \rightarrow {}^3P_2$ transition noticed at around 448 nm has more intense compared to other transitions and it is the advisable excitation wavelength to get intense emission from the PBTNAPr glasses.

The excitation spectra also consist of a broad band in the spectral region from 260 to 350 nm with peak maximum at around 282 nm and sub-peak at around 317 nm. This broad band has been assigned to the absorption of host medium and it is known as host absorption band (HAB) which signifies that the PBTNAPr glasses are inefficient to produce emission when excited at UV radiation. From the excitation spectra, it is also clear that the intensity of observed excitation bands decrease with increase of $PrF_3$ content. The transfer of energy amongst the excited $Pr^{3+}$ ions at higher $PrF_3$ content could be the one of the reasons for decrease in intensity of excitation bands.

#### 3.5.2. Emission spectra

The emission spectra of different contents of $PrF_3$ -doped PBTNAPr glasses were studied by exciting at 448 nm radiation from the xenon flash lamp. The emission spectra normalized w.r.t. the intensity of $^1D_2 \rightarrow {}^3H_4$ transition of PBTNAPr01 glass are shown in Fig. 10. These spectra contain three different sets of emission transitions originating from three different metastable levels, $^3P_1$, $^3P_0$ and $^1D_2$ to various lower lying energy levels. All these transitions are positioned at around 530, 542, 604, 647, 687, 708 and 732 nm corresponding to $^3P_1 \rightarrow {}^3H_5$, $^3P_0 \rightarrow {}^3H_5$, $^1D_2 \rightarrow {}^3H_4$, $^3P_0 \rightarrow {}^3F_2$, $^3P_1 \rightarrow {}^3F_3$, $^3P_1 \rightarrow {}^3F_4$ and $^3P_0 \rightarrow {}^3F_4$ transitions, respectively [32].

It is familiar that the intensity of observed transitions originated from the metastable levels is proportional to their population at different concentrations of $Pr^{3+}$ ions. Among the observed emission transitions, the $^1D_2 \rightarrow {}^3H_4$ transition with peak position at 604 nm has more intense than other transitions and its intensity goes on reduce with the addition of $PrF_3$ content. The variation of intensity of $^1D_2 \rightarrow {}^3H_4$ transition vs. $PrF_3$ content is illustrated in Fig. 11(a). At very low $PrF_3$ contents (nearly 0.1 mol%), the population of $^1D_2$ metastable level increase rapidly due to the rapid-multiphonon relaxation (MPR) rates and non-radiative (NR) relaxation rates from the upper lying $^3P_{2,1,0}$ energy levels. At relatively higher $PrF_3$ contents ($\geq$0.5 mol%), the transfer of energy among the excited $Pr^{3+}$ ions turn into more efficient and dominates the emission intensity resulting fast-quenching in intensity of $^1D_2 \rightarrow {}^3H_4$ transition. The emission spectral profiles also reveal that the intensity of emission bands originated from $^3P_1$ and $^3P_0$ levels (though they are considerably weak) increase with increase of $PrF_3$ content reaches to maximum at $x$ = 0.5 mol% and then reduce for further raise of $PrF_3$ content showing a process known as luminescence quenching. The variation of intensity of $^3P_1 \rightarrow {}^3H_5$ (530 nm) and $^3P_0 \rightarrow$

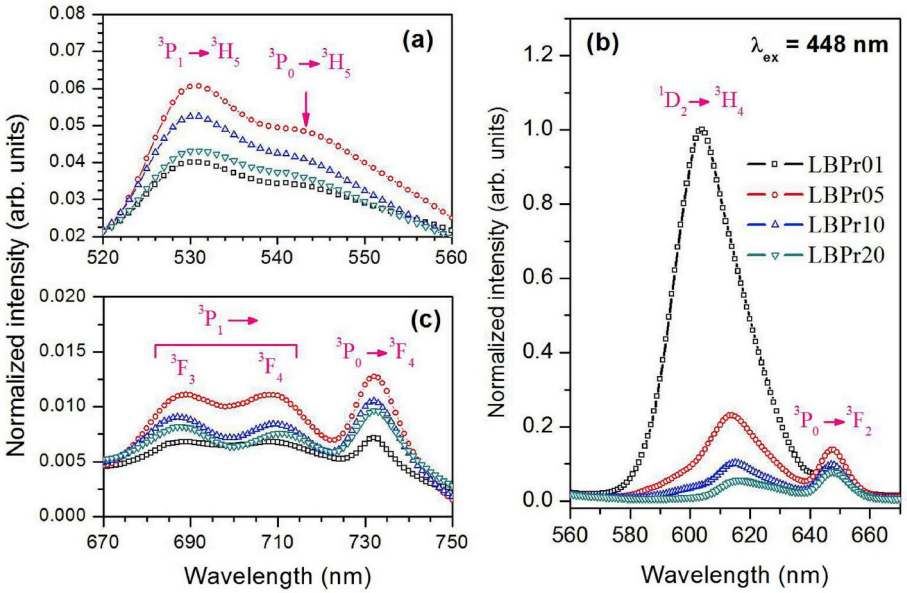


**Fig. 10.** Emission spectra ($\lambda_{ex}$ = 448 nm) of PBTNAPr glasses in the spectral region (a) 520–560 nm, (b) 560–670 nm and (c) 670–750 nm.

$^3F_4$ (732 nm) transitions versus $PrF_3$ content is presented in Fig. 11(b) and (c), respectively. The quenching of luminescence has been ascribed to the increased transfer of energy among the excited $Pr^{3+}$ ions at higher $PrF_3$ contents.

Upon 448 nm excitation, the process of luminescence from the PBTNAPr glasses along with multiphonon relaxation and non-radiative transitions from the upper lying $^3P_{2,1,0}$ energy levels is illustrated in Fig. 12. Further, the position of $^1D_2 \rightarrow {}^3H_4$ transition appears to be shifted from 604 nm to 614 nm when the $PrF_3$ content is raised from 0.1 mol% to 0.5 mol% resulting a red-shift due to a change in site symmetry of the host environment caused by the accumulation of $Pr^{3+}$ ions. For higher contents of $PrF_3$ (i.e., $x$ = 1.0 and 2.0 mol%), the effect of red-shift becomes insignificant due to the uniform distribution of $Pr^{3+}$ ions in the neighborhood of ligand fields [40].

### 3.5.3. Colour perception

The chromaticity of emitted luminescence has been analyzed by evaluating the CIE chromaticity coordinates using the emission spectral profiles. The CIE coordinates are found to be (0.640, 0.360), (0.650, 0.350), (0.645, 0.353) and (0.636, 0.363) for PBTNAPr01, PBTNAPr05, PBTNAPr10 and PBTNAPr20 glasses, respectively. All these coordinates are suitably fitted in rich reddish-orange region of CIE chromaticity diagram and it is shown in Fig. 13. This chromaticity diagram makes known that the PBTNAPr glasses give out the rich reddish-orange emission at 448 nm excitation. These coordinates are very close to LiPbAlB-D (0.630, 0.360) [22] and LTT-B (0.6423, 0.3523) [41] glasses. The emission spectra (see Fig. 10) and the CIE diagram (see Fig. 13) suggest that the PBTNAPr01 glass has great potentiality to produce rich reddish-orange luminescence at 448 nm excitation.

### 3.6. Laser characteristics

The laser characteristic parameters such as experimental branching ratio ($\beta_{exp}$), effective band-width ($\Delta\lambda_{eff}$), stimulated emission cross-section ($\sigma_e$), gain band-width ($\sigma_e \times \Delta\lambda_{eff}$) and optical gain ($\sigma_e \times \tau_{exp}$) have been determined from the radiative properties such as radiative

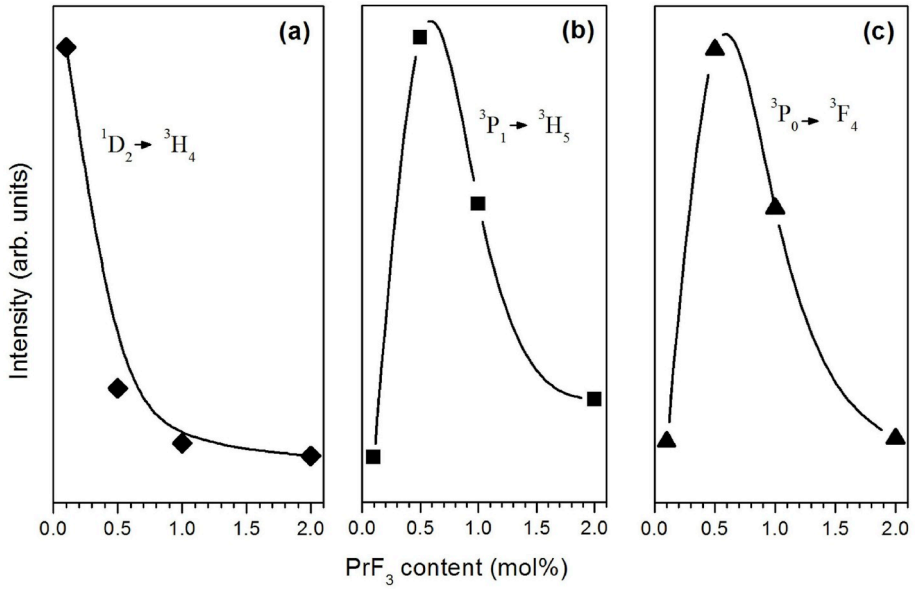


**Fig. 11.** Variation of intensity of $^1D_2 \rightarrow {}^3H_4$ (a), $^3P_1 \rightarrow {}^3H_5$ (b) and $^3P_0 \rightarrow {}^3F_4$ (c) transitions as a function of $PrF_3$ content in PBTNAPr glasses.

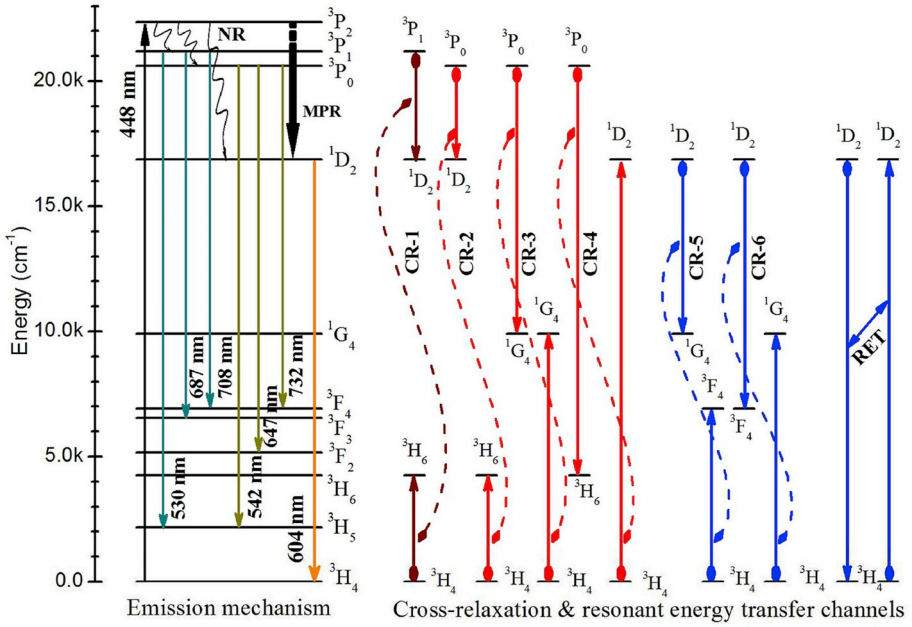


**Fig. 12.** Partial energy level diagram showing the emission mechanism, cross-relaxation channels and resonant energy transfer in PBTNAPr glasses.

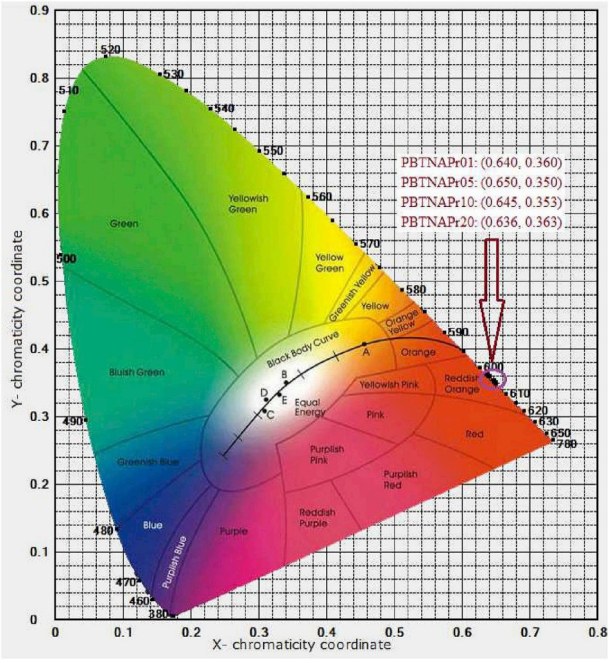


**Fig. 13.** CIE chromaticity diagram for PBTNAPr glasses.

transition probability rate ($A_{rad}$), radiative branching ratio ($\beta_{rad}$) and radiative lifetime ($\tau_{rad}$). According to J-O theory [13,14], the radiative properties for an electric dipole (ED) transition $aJ \rightarrow bJ'$ are given below:

$$A_{rad}(aJ, bJ') = \frac{64\,\pi^4\nu^3}{3h\,(2J+1)}\,\frac{n\,(n^2+2)^2}{9}\,S_{ED} \tag{3}$$

$$\beta_{rad}(aJ, bJ') = A_{rad}(aJ, bJ') \times \tau_{rad}(aJ) \tag{4}$$

$$\tau_{rad} = \left[\sum_{bJ'} A_{rad}(aJ, bJ')\right]^{-1} \tag{5}$$

where $\nu$ is the energy of an upper ($aJ$) manifold level, n is the refractive index of the host medium corresponding to the peak maximum wavelength ($\lambda_P$), J is the total angular momentum of the $aJ$ manifold level and h is the Planck's constant. It is well known fact that the experimental branching ratio ($\beta_{exp}$) should be > 0.50 for intense and high quantum efficiency laser emission and it can be determined from the integrated area under the observed emission bands. A comparison of radiative properties of $^1D_2 \rightarrow {}^3H_4$ transition is shown in Table 7.

The stimulated emission cross-section ($\sigma_e$) of an emission transition ($aJ \rightarrow bJ'$) has been evaluated using the following equation [13,14].

$$\sigma_e(aJ, bJ') = \frac{\lambda_p^4}{8\,\pi\,c\,n^2\,\Delta\lambda_{eff}}\,A_{rad}(aJ, bJ') \tag{6}$$

where $\lambda_P$, $c$ and $\Delta\lambda_{eff}$ are known as the peak-maximum wavelength, the speed of light and the effective bandwidth, respectively. The observed values of experimental branching ratio, effective band-width, stimulated emission cross-section, gain band-width and optical gain for the studied glass-samples are summarized in Table 8. The evaluated laser characteristic parameters of PBTNAPr01 glass are close to those reported for SFB:1.0$Pr^{3+}$ [7], PbO–$H_3BO_3$–$TiO_2$–$AlF_3$ [8], LiPbAlB–F [22] and ZnAlBiB-A [42] glasses. A comparison of laser characteristic parameters for different glass samples is given in Table 9.

**Table 7**
Comparison of radiative properties of $^1D_2 \rightarrow {}^3H_4$ transition in PBTNAPr glasses.

| Parameter | PBTNAPr01 | PBTNAPr05 | PBTNAPr10 | PBTNAPr20 |
|---|---|---|---|---|
| Energy of $^1D_2$ level ($\nu$, cm$^{-1}$) | 16556 | 16287 | 16287 | 16287 |
| Radiative transition rate ($A_{rad}$, s$^{-1}$) | 371 | 405 | 397 | 372 |
| Radiative branching ratio ($\beta_{rad}$) | 0.43 | 0.40 | 0.38 | 0.33 |
| Experimental branching ratio ($\beta_{exp}$) | 0.98 | 0.85 | 0.69 | 0.52 |
| Radiative lifetime ($\tau_{rad}$, μ s) | 1148 | 994 | 950 | 892 |

**Table 8**
Laser characteristics parameters such as emission peak position ($\lambda_P$, nm), effective bandwidth ($\Delta\lambda_{eff}$, nm), stimulated emission cross-section ($\sigma_e$), gain bandwidth ($\sigma_e \times \Delta\lambda_{eff}$) and optical gain ($\sigma_e \times \tau_{exp}$) for $^1D_2 \rightarrow {}^3H_4$ transition in PBTNAPr glasses.

| Parameter | PBTNAPr01 | PBTNAPr05 | PBTNAPr10 | PBTNAPr20 |
|---|---|---|---|---|
| $\lambda_P$, nm | 604 | 614 | 614 | 614 |
| $\Delta\lambda_{eff}$, nm | 18.31 | 27.59 | 26.16 | 25.49 |
| $\sigma_e \times 10^{-22}$ cm$^2$ | 14.968 | 11.438 | 11.675 | 11.112 |
| $(\sigma_e \times \Delta\lambda_{eff}) \times 10^{-27}$ cm$^3$ | 2.741 | 3.156 | 3.054 | 2.832 |
| $(\sigma_e \times \tau_{exp}) \times 10^{-24}$ cm$^2$-s | 1.510 | 0.511 | 0.420 | 0.343 |

### 3.7. Luminescence decay analysis

#### 3.7.1. Estimation of lifetime

The lifetime of $Pr^{3+}$: $^1D_2$ metastable level in PBTNAPr glasses is measured monitoring the emission and excitation wavelengths at 604 and 448 nm, respectively. The decay profiles of PBTNAPr glasses are described in Fig. 14. The decay pattern of PBTNAPr01 glass is suitably fitted to single-exponential function, $I_t = I_0 . \exp\left(\frac{-t}{\tau}\right)$, where $I_o$ is the initial luminescence intensity (i.e., when t = 0) and $\tau$ is the lifetime of the emission level. The experimental lifetime ($\tau_{exp}$) is obtained by taking the first e-folding times of the initial intensity of decay profile. The single-exponential fitting of decay curves is an indication for the absence of non-radiative decay rates. For PBTNAPr01 glass, the experimental lifetime is estimated to be 1009 μs.

Since the decay profiles of PBTNAPr05, PBTNAPr10 and PBTNAPr20 glasses deviate from exponential to non-exponential nature, the lifetime is estimated by fitting them to double exponential function, $I_t = A_1 . e^{-t/\tau_1} + A_2 . e^{-t/\tau_2}$, where $I_t$ is the initial intensity at t = 0 s and $\tau_1$ and $\tau_2$ represents the lifetimes for long (slow) and short (fast) decay components. The average lifetime, $\langle\tau\rangle$ has been obtained using the following relation.

$$\langle\tau\rangle = \frac{A_1\tau_1^2 + A_2\tau_2^2}{A_1\tau_1 + A_2\tau_2} \quad (7)$$

The values of $\langle\tau\rangle$ are found to be 447, 360 and 309 μs for PBTNAPr05, PBTNAPr10 and PBTNAPr20 glasses, respectively. The experimental lifetimes are found to decrease with increase of $PrF_3$ content due to increased non-radiative decay processes through the transfer of energy initiated by various interaction mechanisms among the excited $Pr^{3+}$ ions. The inset of Fig. 14 shows the variation of lifetime as a function of $PrF_3$ content.

#### 3.7.2. Non-radiative decay rates

The phenomena of quenching in luminescence and the shortening in lifetime values with increase of concentration of active ions are due to the non-radiative decay rates ($W_{NR}$) from the metastable level to its lower lying energy levels and the migration of energy among the excited active ions. The non-radiative decay rates are given as, $W_{NR} = W_{MPR} + W_{ET} + W_{CQ} + W_{OH}$, where $W_{MPR}$, $W_{ET}$, $W_{CQ}$ and $W_{OH}$ represents the non-radiative rates due to multiphonon-relaxation, energy transfer, concentration quenching and the presence of $OH^-$ content, respectively. In the present investigation, the non-radiative decay rates due to $OH^-$ content become insignificant owing to considerably small value of coefficient of $OH^-$ (~66.81 ppm). Since the

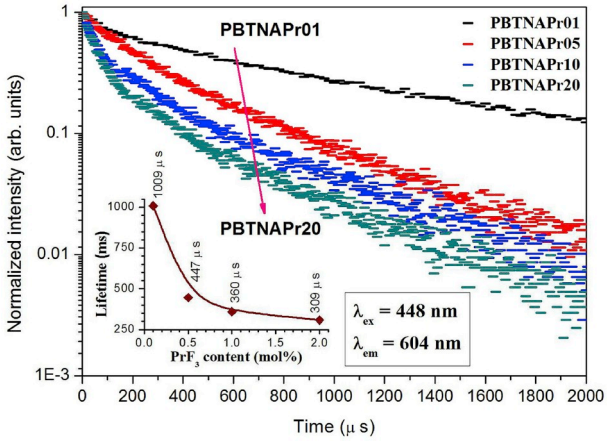


**Fig. 14.** Luminescence decay patterns of $Pr^{3+}$: $^1D_2$ emission level in PBTNAPr glasses.

phonon energy of PBTNAPr glasses is of the order of ~1005 cm$^{-1}$, nearly seven phonons are required to bridge the energy difference (~6952 cm$^{-1}$) between the $^1D_2$ metastable level and its immediate lower lying $^1G_4$ quantum level. Thus, the multiphonon-relaxation, energy transfer and concentration quenching non-radiative rates play a significant role in luminescence quenching as well as lifetime shortening. The effective non-radiative decay rates can be written as

$$W_{NR} = W_{MPR} + W_{ET} + W_{CQ} = \frac{1}{\tau_{exp}} - \frac{1}{\tau_{rad}} \quad (8)$$

The non-radiative decay rates are found to be 120, 1231, 1725 and 2115 cm$^{-1}$ for PBTNAPr01, PBTNAPr05, PBTNAPr10 and PBTNAPr20 glasses, respectively. These results indicate that the $W_{NR}$ becomes insignificant for PBTNAPr01 glass leading to fit single-exponential function. From the literature [43,44] it is known that an overlap of absorption and emission spectra results a resonant energy transfer (RET) among the excited active ions. The spectral overlap between absorption ($^3H_4 \rightarrow {}^1D_2$) and emission ($^1D_2 \rightarrow {}^3H_4$) transitions of $Pr^{3+}$ ions in PBTNAPr glasses is presented in Fig. 15. This spectral overlap leads energy migration from excited to unexcited $Pr^{3+}$ ions through resonant energy transfer process. The non-radiative decay rates at higher contents of $PrF_3$ ($x \geq 0.5$ mol%) can be ascribed to various cross-relaxation (CR) and resonant energy transfer (RET) channels shown below and they are illustrated in Fig. 12.

**Table 9**
Comparison of laser characteristics parameters of $^1D_2 \rightarrow {}^3H_4$ transition in different multi-component glasses.

| Parameter | PBTNAPr01 [Present work] | LiPbAlB–F [22] | ZnAlBiB-A [42] | PbO–$H_3BO_3$–$TiO_2$–$AlF_3$ [8] | SFB:1.0$Pr^{3+}$ [7] |
|---|---|---|---|---|---|
| $\lambda_P$, nm | 604 | 602 | 603 | 604 | 603 |
| $\Delta\lambda_{eff}$, nm | 18.31 | 23.06 | 28.2 | 17.46 | 20 |
| $\beta_{exp}$ | 0.98 | 0.54 | 0.284 | 0.74 | 0.32 |
| $\sigma_e \times 10^{-22}$ cm$^2$ | 14.968 | 13.6 | 15.5 | 13.0 | 2.21 |
| $(\sigma_e \times \Delta\lambda_{eff}) \times 10^{-27}$ cm$^3$ | 2.741 | 3.1 | 4.3 | 2.27 | 0.78 |
| $(\sigma_e \times \tau_{exp}) \times 10^{-24}$ cm$^2$-s | 1.510 | 0.396 | 0.424 | 0.54 | 3.09 |

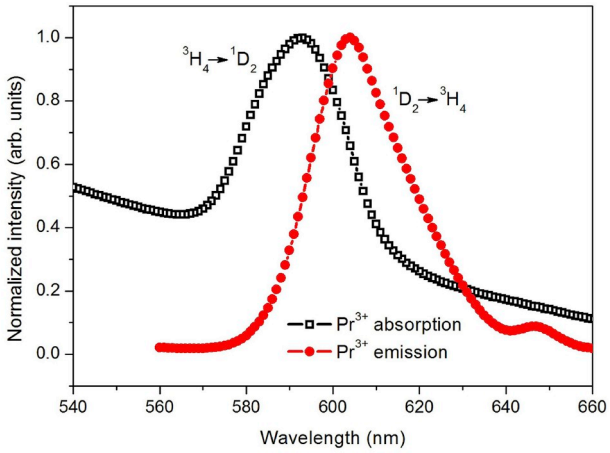


**Fig. 15.** Spectral overlap of absorption ($^3H_4 \rightarrow {}^1D_2$) and emission ($^1D_2 \rightarrow {}^3H_4$) transitions of $Pr^{3+}$ ions in PBTNAPr glasses.

| CR channel | Donor emission channel | Acceptor absorption channel |
|---|---|---|
| CR-1: | $^3P_1 \rightarrow {}^1D_2$ (4323 $cm^{-1}$) | $^3H_4 \rightarrow {}^3H_6$ (4241 $cm^{-1}$) |
| CR-2: | $^3P_0 \rightarrow {}^1D_2$ (3755 $cm^{-1}$) | $^3H_4 \rightarrow {}^3H_6$ (4241 $cm^{-1}$) |
| CR-3: | $^3P_0 \rightarrow {}^1G_4$ (10707 $cm^{-1}$) | $^3H_4 \rightarrow {}^1G_4$ (9911 $cm^{-1}$) |
| CR-4: | $^3P_0 \rightarrow {}^3H_6$ (16373 $cm^{-1}$) | $^3H_4 \rightarrow {}^1D_2$ (16863 $cm^{-1}$) |
| CR-5: | $^1D_2 \rightarrow {}^1G_4$ (6952 $cm^{-1}$) | $^3H_4 \rightarrow {}^3F_4$ (6920 $cm^{-1}$) |
| CR-6: | $^1D_2 \rightarrow {}^3F_4$ (9943 $cm^{-1}$) | $^3H_4 \rightarrow {}^1G_4$ (9911 $cm^{-1}$) |
| RET: | $^1D_2 \rightarrow {}^3H_4$ (16863 $cm^{-1}$) | $^3H_4 \rightarrow {}^1D_2$ (16863 $cm^{-1}$) |

### 3.7.3. Non-exponential decay

The non-exponentiality of decay profiles of $Pr^{3+}$: $^1D_2$ metastable level in PBTNAPr glasses at higher contents of $PrF_3$ ($x \geq 0.5$ mol%) could be due to a mixture of interaction mechanisms involved among the excited $Pr^{3+}$ ions and it can be studied applying the Inokuti-Hirayama (I–H) model [45]. This model proposed a relation for variation of luminescence intensity with time and it is given as

$$I_t = I_0 . \exp\left\{-\left(\frac{t}{\tau_0}\right) - Q\left(\frac{t}{\tau_0}\right)^{3/S}\right\} \quad (9)$$

where $\tau_0$ is the intrinsic lifetime, $I_o$ is the luminescence intensity at t = 0 s, Q is the energy transfer parameter and S is the interaction parameter which is equal to 3 for exchange interaction, 6 for dipole-dipole (d-d) interaction, 8 for dipole-quadrupole (d-q) interaction and 10 for quadrupole-quadrupole (q-q) interaction. The energy transfer parameter involves concentration of RE ions (N), critical transfer distance ($R_0$) between the donor and acceptor ions at which the rate of energy transfer is numerically equal to reciprocal of intrinsic lifetime ($\tau_0$) and Euler's function ($\Gamma$) which is equal to 6 for d-d interaction, 8 for d-q interaction and 10 for q-q interaction. The value of Q has been determined using the following equation.

$$Q = \frac{4\pi}{3} . \Gamma\left(1 - \frac{3}{S}\right) . N . R_0^3 \quad (10)$$

In the present investigation, the intrinsic lifetime is found to be ~1009 μs□ The decay profiles for $x \geq 0.5$ mol% have been fitted to S = 6 (not shown) confirming the energy transfer through d-d interaction mechanism. Further, the donor-acceptor interaction parameter, $C_{DA}$ ($= R_0^S/\tau_0$) plays a significant role in studying the mechanism of transfer of energy among the excited $Pr^{3+}$ ions at higher contents of $PrF_3$. The values of energy transfer parameter, critical transfer distance and donor–acceptor interaction parameter are summarized in Table 10. The increase of energy transfer parameter and the decrease of critical transfer distance and donor–acceptor interaction parameter with the addition of $PrF_3$ content supports the improved non-radiative decay rates and the deviation of exponential nature to non-exponential for PBTNAPr05, PBTNAPr10 and PBTNAPr20 glasses. Similar kind of results was reported for LiPbAlB glasses [22].

**Table 10**
Experimental ($\tau_{exp}$) and radiative ($\tau_{rad}$) lifetimes, quantum efficiencies ($\eta_{QE}$), non-radiative decay rates ($W_{NR}$), energy transfer parameters ($Q_{ET}$), critical transfer distances ($R_0$) and donor–acceptor interaction parameters ($C_{DA}$) for $^1D_2 \rightarrow {}^3H_4$ transition in PBTNAPr glasses.

| Parameter | PBTNAPr01 | PBTNAPr05 | PBTNAPr10 | PBTNAPr20 |
|---|---|---|---|---|
| $\tau_{exp}$ (μ s) | 1009 | 447 | 360 | 309 |
| $\tau_{rad}$ (μ s) | 1148 | 994 | 950 | 892 |
| $\eta_{QE}$ (%) | 85 | 45 | 38 | 35 |
| $W_{NR}$ ($s^{-1}$) | 120 | 1231 | 1725 | 2115 |
| $Q_{ET}$ | – | 1.29 | 1.58 | 2.54 |
| $R_0$ (nm) | – | 0.243 | 0.206 | 0.192 |
| $C_{DA}$ ( $\times 10^{-42}$ $cm^6/s$) | – | 2.041 | 0.761 | 0.499 |

### 3.7.4. Quantum efficiency

In order to know the applicability of prepared glassy materials as laser hosts one must know their quantum efficiency ($\eta_{QE}$) and it can be evaluated from the experimental and radiative lifetimes.

$$\eta_{QE} = \frac{\tau_{exp}}{\tau_{rad}} \quad (11)$$

The values of $\eta_{QE}$ are found to be 87%, 45%, 38% and 35% for PBTNAPr01, PBTNAPr05, PBTNAPr10 and PBTNAPr20 glasses, respectively. It can also be estimated from the experimentally obtained luminescence peak intensity and lifetime [46] using the following equation.

$$\eta_{QE} = \frac{1}{\tau} \int I(t) . dt \quad (12)$$

According to Eq. (12), the value of $\eta_{QE}$ is found to be 88% for PBTNAPr01 glass and it is similar to that obtained from Eq. (11). The quantum efficiency of PBTNAPr01 glass is comparable to LiPbAlB-D (86%) [22] glass and found higher than PbWTe–B (75.3%) [3], PTBPr01 (66%) [6] and TeWK (72.5%) [47] glasses. The experimentally obtained results reveal that the PBTNAPr01 glass has great potentiality to design a new and novel laser emitting rich reddish-orange luminescence. The laser characteristic properties of PBTNAPr glasses with $x < 0.1$ mol% and the effect of sensitizers on the luminescence of $Pr^{3+}$ ions will be discussed in near future.

## 4. Conclusions

The PBTNAPr glasses containing different amounts (in mol%) of $PrF_3$ have been prepared and analyzed for laser applications. They are thermally more stable and they have superior glass-forming tendency without devitrification. The formation of various functional units such as B–O asymmetric stretching vibrations, B–O–B bending vibrations and Pb–O vibrational units confirms the presence of lead and borate structural units. Considerably small phonon energy and coefficient of $OH^-$ are found to be 1005 $cm^{-1}$ and 66.81 ppm, respectively. The covalent character of nearly 57% results considerably large rigidity and it decrease slightly with increase of $PrF_3$ content due to structural modifications. The direct allowed optical band gap energy is found to be nearly 2.445 eV for PBTNAPr01 glass. The modified J-O theory has been applied by modifying the electric dipole linestrengths to evaluate various spectroscopic and laser characteristic properties. The emission profiles observed at 448 nm excitation show luminescence quenching due to energy transfer among the excited $Pr^{3+}$ ions at higher $PrF_3$ contents. The decay profiles at higher $PrF_3$ content (≥0.5 mol %) deviate from exponential to non-exponential nature and it has been well fitted to I–H model for dipole-dipole interaction mechanism. The quantum efficiency of $^1D_2$ metastable level has been estimated to be 87%. The observed results suggest that the PBTNAPr01 glass has more potential for rich orange-red laser applications.

## Declaration of competing interest

The authors declare that they have no known competing financial interests or personal relationships that could have appeared to influence the work reported in this paper.

## Acknowledgments

Dr. B.C. Jamalaiah acknowledges the financial assistance from UGC-SERO, Hyderabad (F·NO:4-4/2015-16(MRP/UGC-SERO), Dated: October 2016) and SERB-DST, New Delhi (File No. EMR/2016/007217, Dated: 18 May 2017). Dr. G. Viswanadha is also thankful to the SERB-DST for the financial support through Junior Research Fellow (JRF).

## References

[1] J. Zhao, L. Huang, T. Liang, S. Zhao, S. Xu, Luminescent properties of $Eu^{3+}$ doped heavy tellurite scintillating glasses, J. Lumin. 205 (2019) 342–345 https://doi.org/10.1016/j.jlumin.2018.09.045.

[2] O. Kıbrıslı, A.E. Ersundu, M. Çelikbilek Ersundu, $Dy^{3+}$ doped tellurite glasses for solid-state lighting: an investigation through physical, thermal, structural and optical spectroscopy studies, J. Non-Cryst. Solids 513 (2019) 125–136 https://doi.org/10.1016/j.jnoncrysol.2019.03.020.

[3] R. Sharma, A.S. Rao, N. Deopa, M. Venkateswarlu, M. Jayasimhadri, D. Haranath, G.V. Prakash, Spectroscopic study of $Pr^{3+}$ ions doped zinc lead tungsten tellurite glasses for visible photonic device applications, Opt. Mater. 78 (2018) 457–464 https://doi.org/10.1016/j.optmat.2018.02.054.

[4] K.V. Krishnaiah, E.S. de Lima Filho, Y. Ledemi, G. Nemova, Y. Messaddeq, R. Kashyap, Development of ytterbium-doped oxyfluoride glasses for laser cooling applications, Nat. Sci. Rep. 6 (2016) 21905 https://doi.org/10.1038/srep21905.

[5] K.V. Krishnaiah, Y. Ledemi, C. Genevois, E. Veron, X. Sauvage, S. Morency, E.S. de Lima Filho, G. Nemova, M. Allix, Y. Messaddeq, R. Kashyap, Ytterbium-doped oxyfluoride nano-glass-ceramic fibers for laser cooling, Opt. Mater. Express 7 (2017) 1980–1994 https://doi.org/10.1364/OME.7.001980.

[6] M.V.V. Kumar, K.R. Gopal, R.R. Reddy, G.V.L. Reddy, N.S. Hussain, B.C. Jamalaiah, Application of modified Judd–Ofelt theory and the evaluation of radiative properties of $Pr^{3+}$ -doped lead telluroborate glasses for laser applications, J. Non-Cryst. Solids 364 (2013) 20–27 https://doi.org/10.1016/j.jnoncrysol.2012.11.049.

[7] D. Umamaheswari, B.C. Jamalaiah, T. Chengaiah, I.G. Kim, L.R. Moorthy, Optical properties of sodium fluoroborate glasses containing $Pr^{3+}$ ions for red luminescence, Phys. Chem. Glasses Eur. J. Glass Sci. Technol. B 53 (2012) 271–275 https://www.ingentaconnect.com/content/sgt/ejgst/2012/00000053/00000006/art00005.

[8] B.C. Jamalaiah, J.S. Kumar, A.M. Babu, L.R. Moorthy, K. Jang, H.S. Lee, M. Jayasimhadri, J.H. Jeong, H. Choi, Optical absorption, fluorescence and decay properties of $Pr^{3+}$ -doped PbO-$H_3BO_3$-$TiO_2$-$AlF_3$ glasses, J. Lumin. 129 (2009) 1023–1028 https://doi.org/10.1016/j.jlumin.2009.04.018.

[9] J.S. Wang, E.M. Vogel, E. Snitzer, Tellurite glass: a new candidate for fiber devices, Opt. Mater. 3 (1994) 187–203 https://doi.org/10.1016/0925-3467(94)90004-3.

[10] D. Rajesh, $Pr^{3+}$ doped new TZYN glasses and glass-ceramics containing $NaYF_4$ nanocrystals: luminescence analysis for visible and NIR applications, Opt. Mater. 86 (2018) 178–184 https://doi.org/10.1016/j.optmat.2018.10.004.

[11] C. Lu, H. Guo, Y. Xu, C. Hou, M. Lu, X. He, P. Wang, W. Li, B. Peng, Mid-infrared emissions of $Pr^{3+}$-doped $GeS_2$-$Ga_2S_3$-$CdI_2$ chalcohalide glasses, Mater. Res. Bull. 60 (2014) 391–396 https://doi.org/10.1016/j.materresbull.2014.09.003.

[12] K. Wei, D.P. Machewirth, J. Wenzel, E. Snitzer, G.H. Sigel Jr., $Pr^{3+}$ -doped Ge-Ga-S glasses for 1.3 μm optical fiber amplifiers, J. Non-Cryst. Solids 182 (1995) 257–261 https://doi.org/10.1016/0022-3093(94)00513-3.

[13] B.R. Judd, Optical absorption intensities of rare-earth ions, Phys. Rev. 127 (1962) 750–761 https://doi.org/10.1103/PhysRev.127.750.

[14] G.S. Ofelt, Intensities of crystal spectra of rare-earth ions, J. Chem. Phys. 37 (1962) 511–520 https://doi.org/10.1063/1.1701366.

[15] B.C. Jamalaiah, $GeO_2$ activated tellurite tungstate glass: a new candidate for solid state lasers and fiber devices, J. Non-Cryst. Solids 502 (2018) 54–61 https://doi.org/10.1016/j.jnoncrysol.2018.03.032.

[16] A. Hruby, Evolution of glass-forming tendency by means of DTA, Czech, J. Physiol. Biochem. 22 (1972) 1187–1193 https://doi.org/10.1007/BF01690134.

[17] Y. Yang, B. Chen, C. Wang, G. Ren, Q. Meng, X. Zhao, W. Di, X. Wang, J. Sun, L. Cheng, T. Yu, Y. Peng, Spectroscopic properties of $Er^{3+}$ -doped $x$$GeO_2$-(80-$x$)$TeO_2$-10ZnO-10BaO glasses, J. Non-Cryst. Solids 354 (2008) 3747–3751 https://doi.org/10.1016/j.jnoncrysol.2008.03.047.

[18] V. Naresh, B.S. Ham, Influence of multiphonon and cross relaxations on $^3P_0$ and $^1D_2$ emission levels of $Pr^{3+}$ doped borosilicate glasses for broad band signal amplification, J. Alloy. Comp. 664 (2016) 321–330 https://doi.org/10.1016/j.jallcom.2015.12.246.

[19] S. Hong-Tao, D. Shi-Xun, X. Shi-Qing, H. Li-Li, J. Zhong-Hong, Frequency upconversion emission of $Er^{3+}$ -doped strontium-lead-bismuth glasses, Chin. Phys. Lett. 21 (2004) 2292–2294 http://iopscience.iop.org/0256-307X/21/11/060.

[20] R. Ciceo-Lucacel, L. Ardelean, FT-IR and Raman study of silver lead borate-based glasses, J. Non-Cryst. Solids 353 (2007) 2020–2024 https://doi.org/10.1016/j.jnoncrysol.2007.01.066.

[21] S. Rada, M. Culea, M. Neumann, E. Culea, Structural role of europium ions in lead–borate glasses inferred from spectroscopic and DFT studies, Chem. Phys. Lett. 460 (2008) 196–199 https://doi.org/10.1016/j.cplett.2008.05.088.

[22] N. Deopa, A.S. Rao, Sk Mahamuda, M. Gupta, M. Jayasimhadri, D. Haranath, G.V. Prakash, Spectroscopic studies of $Pr^{3+}$ doped lithium lead alumino borate glasses for visible reddish orange luminescent device applications, J. Alloy. Comp. 708 (2017) 911–921 https://doi.org/10.1016/j.jallcom.2017.03.020.

[23] M.V.V. Kumar, B.C. Jamalaiah, K.R. Gopal, R.R. Reddy, Optical absorption and fluorescence studies of $Dy^{3+}$ -doped lead telluroborate glasses, J. Lumin. 132 (2012) 86–90 https://doi.org/10.1016/j.jlumin.2011.07.021.

[24] J. Pisarska, W.A. Pisarski, W. Ryba-Romanowski, Laser spectroscopy of $Nd^{3+}$ and $Dy^{3+}$ ions in lead borate glasses, Opt. Laser. Technol. 42 (2010) 805–809 https://doi.org/10.1016/j.optlastec.2009.12.008.

[25] J. Pisarska, Luminescence behavior of $Dy^{3+}$ ions in lead borate glasses, Opt. Mater. 31 (2009) 1784–1786 https://doi.org/10.1016/j.optmat.2008.11.028.

[26] H.E. Heidepriem, W. Seeber, D. Ehrt, Dehydration of phosphate glasses, J. Non-Cryst. Solids 163 (1993) 74–80 https://doi.org/10.1016/0022-3093(93)90647-G.

[27] K. Swapna, Sk Mahamuda, A.S. Rao, S. Shakya, T. Sasikala, D. Haranath, G.V. Prakash, Optical studies of $Sm^{3+}$ ions doped zinc alumino bismuth borate glasses, Spectrochim. Acta A Mol. Biomol. Spectrosc. 125 (2014) 53–60 https://doi.org/10.1016/j.saa.2014.01.025.

[28] B.C. Jamalaiah, T. Suhasini, L.R. Moorthy, I.G. Kim, D.S. Yoo, K.W. Jang, Structural and luminescence properties of $Nd^{3+}$-doped PbO–$B_2O_3$–$TiO_2$–$AlF_3$ glass for 1.07 μm laser applications, J. Lumin. 132 (2012) 1144–1149 https://doi.org/10.1016/j.jlumin.2011.12.073.

[29] T. Som, B. Karmakar, Nephelauxetic effect of low phonon antimony oxide glass in absorption and photoluminescence of rare-earth ions, Spectrochim. Acta A Mol. Biomol. Spectrosc. 79 (2011) 1766–1782 https://doi.org/10.1016/j.saa.2011.05.054.

[30] B.B. Kale, A. Jha, S.K. Apte, V. Adhyapak, D.P. Amalnerkar, Removal of OH impurities from $GeS_2$ by reactive atmosphere and its glass preparation, Mater. Chem. Phys. 78 (2002) 330–336 https://doi.org/10.1016/S0254-0584(01)00551-X.

[31] T.I. Suratwala, R.A. Steele, G.D. Wilke, J.H. Campbell, K. Takeuchi, Effects of OH content, water vapor pressure, and temperature on sub-critical crack growth in phosphate glass, J. Non-Cryst. Solids 78 (2002) 213–227 https://doi.org/10.1016/S0022-3093(99)00680-8.

[32] W.T. Carnall, P.R. Fields, K. Rajnak, Electronic energy levels in the trivalent lanthanide aquo ions. I. $Pr^{3+}$, $Nd^{3+}$, $Pm^{3+}$, $Sm^{3+}$, $Dy^{3+}$, $Ho^{3+}$, $Er^{3+}$ and $Tm^{3+}$, J. Chem. Phys. 49 (1968) 4424–4442 https://doi.org/10.1063/1.1669893.

[33] S.P. Sinha, H.H. Schmidtke, The nephelauxetic effect in rare earth complexes illustrated for praseodymium (III), Mol. Phys. 10 (1965) 7–11 https://doi.org/10.1080/00268976600100021.

[34] L. Pauling, The Nature of Chemical Bond - an Introduction to Modern Structural Chemistry, third ed., Cornell University Press, Ithaca, New York, 10-13.

[35] N.F. Mott, E.A. Davis, Electronic Processes in Non-crystalline Materials, second ed., Clarendon Press, New York, 1979, pp. 382–428.

[36] W.T. Carnall, The absorption and fluorescent spectra of rare earth ions in solution, in: K.A. Gschneidner, L. Eyring (Eds.), Handbook on the Physics and Chemistry of Rare Earths, vol 3, North-Holland, Amsterdam, 1979, pp. 171–208 C-24.

[37] A.A. Kornienko, A.A. Kaminskii, E.B. Dunina, Dependence of the line strength of f–f transitions on the manifold energy. II. Analysis of $Pr^{3+}$ in $KPrP_4O_{12}$, Phys. Status Solidi B 157 (1990) 267–273 https://doi.org/10.1002/pssb.2221570127.

[38] A. Herrera, C. Jacinto, A.R. Becerra, P.L. Franzen, N.M. Balzaretti, Multichannel emission from $Pr^{3+}$ doped heavy-metal oxide glass $B_2O_3$-PbO-$GeO_2$-$Bi_2O_3$ for broadband signal amplification, J. Lumin. 180 (2016) 341–347 https://doi.org/10.1016/j.jlumin.2016.08.019.

[39] P. Srivastava, S.B. Rai, D.K. Rai, Effect of lead oxide on optical properties of $Pr^{3+}$ doped some borate based glasses, J. Alloy. Comp. 368 (2004) 1–7 https://doi.org/10.1016/S0925-8388(03)00742-4.

[40] X.J. Wang, H.R. Zheng, D. Jia, S.H. Huang, R.S. Meltzer, M.J. Dejneka, W.M. Yen, Spectroscopy of different sites in $Pr^{3+}$ -doped oxyfluoride glass ceramics, Microelectron. J. 34 (2003) 549–551 https://doi.org/10.1016/S0026-2692(03)00045-4.

[41] M. Venkateswarlu, M.V.V.K.S. Prasad, K. Swapna, Sk Mahamuda, A.S. Rao, A.M. Babu, D. Haranath, $Pr^{3+}$ doped lead tungsten tellurite glasses for visible red lasers, Ceram. Int. 40 (2014) 6261–6269 https://doi.org/10.1016/j.ceramint.2013.11.084.

[42] Sk Mahamuda, K. Swapna, A.S. Rao, T. Sasikala, L.R. Moorthy, Reddish-orange emission from $Pr^{3+}$ doped zinc alumino bismuth borate glasses, Physica B 428 (2013) 36–42 https://doi.org/10.1016/j.physb.2013.07.010.

[43] D.L. Dexter, A theory of sensitized luminescence in solids, J. Chem. Phys. 21 (1953) 836–850 https://doi.org/10.1063/1.1699044.

[44] D.L. Dexter, J.H. Schulman, Theory of concentration quenching in inorganic phosphors, J. Chem. Phys. 22 (1954) 1063–1070 https://doi.org/10.1063/1.1740265.

[45] M. Inokuti, F. Hirayama, Influence of energy transfer by the exchange mechanism on donor luminescence, J. Chem. Phys. 43 (1965) 1978–1989 https://doi.org/10.1063/1.1697063.

[46] K.B. Eisenthal, S. Siegal, Influence of resonance transfer on luminescence decay, J. Chem. Phys. 41 (1964) 652–655 https://doi.org/10.1063/1.1725941.

[47] C.B.A. Devi, Sk Mahamuda, K. Swapna, M. Venkateswarlu, A.S. Rao, G.V. Prakash, $Pr^{3+}$ ions doped single alkali and mixed alkali fluoro tungsten tellurite glasses for visible red luminescent devices, J. Non-Cryst. Solids 498 (2018) 345–351 https://doi.org/10.1016/j.jnoncrysol.2018.03.034.